THIRD EUROPEAN ROTORCRAFT AND POWERED LIFT AIRCRAFT FORUM

Paper No 17

FLIGHT EXPERIMENTS ON AERODYNAMIC FEATURES AFFECTING HELICOPTER BLADE DESIGN

P. BROTHERHOOD AND M. J. RILEY

RAE, FARNBOROUGH, UK

September 7-9, 1977

AIX-EN-PROVENCE, FRANCE

ASSOCIATION AERONAUTIQUE ET ASTRONAUTIQUE DE FRANCE

FLIGHT EXPERIMENTS ON AERODYNAMIC FEATURES AFFECTING HELICOPTER BLADE DESIGN

P. BROTHERHOOD AND M. J. RILEY

RAE, FARNBOROUGH

1 INTRODUCTION

A major part of a continuing programme of helicopter flight research at the Royal Aircraft Establishment, Bedford is devoted to the aerodynamics of the main rotor. This flight research forms part of an integrated research programme within RAE which includes theoretical work and wind tunnel tests on rotor aerodynamics together with parallel work in structural dynamics and allied topics. Close liaison is maintained with Westland Helicopters Ltd on all aspects of the work.

Much of the earlier flight research described in this paper has been carried out using a Westland Wessex as the test vehicle but our current programme utilises a Puma helicopter. A major part of our work has been concerned with detailed measurement and comparison of aerofoil characteristics, that is blade chordwise pressure distributions in hovering and forward flight, and profile drag in hovering flight[1], at a single radial station near the rotor tip. Recent tests made on the Puma by contrast have concentrated on detailed measurements of radial pressure distributions along the leading and trailing edges of the blade as indicators of local incidence and stall.

The tests were flown systematically to examine whenever possible the basic helicopter phenomenon of retreating blade stall, stall flutter, blade-vortex interaction and advancing blade compressibility effects. A large body of data has been recorded on magnetic tape and extensive computer programs written so that the data can be readily retrieved and assessed in graphical form on a Visual Display Unit and hard copied as required. Even so the amount and varied nature of the results has meant that inevitably only a small part of the available data has so far been studied in detail.

Other tests of a somewhat different nature have included the effects on performance and loads of leading edge roughness applied to simulate leading edge erosion[2]. These tests have led to the use of leading edge roughness in a controlled way to investigate the spanwise lift requirements of a helicopter blade[3].

This paper summarises very briefly three experiments made on the Wessex and Puma helicopters commenting where appropriate on particular features affecting helicopter blade design. As the techniques used in the investigation of spanwise lift requirements are somewhat novel, these tests are described first.

2 INVESTIGATION OF THE SPANWISE LIFT REQUIREMENTS OF A HELICOPTER BLADE.

Previous tests showed that leading edge roughness of a degree comparable to moderate erosion of unprotected light alloy blades initiated premature blade stall and characteristic changes in the signature of blade torsional load. It was realised that artificially roughening the leading edge of the rotor blades would be a convenient way of making changes in the distribution of achievable lift coefficient along the blade. Used in this way, locally applied roughness provides an experimental tool to investigate the requirements for tailoring blade section design in order to raise the limits of rotor performance.

One of the factors which limits the performance of a rotor is blade stall on the retreating blade side of the rotor disc. Cambered sections can be used to improve the lifting ability of the blade but their large inherent pitching moments generate excessive control loads due to the high velocity on the advancing side of the rotor disc. This tends to preclude the use of highly cambered sections over the entire blade radius.

In discussion with Westland Helicopters Ltd it was decided to investigate two aspects of this design problem. The first concerns the use of reflex cambered profiles inboard on the blade to offset the pitching moments generated by the profiles with positive camber used further outboard. The second was to explore the maximum lift coefficient requirements of the blade tip region in the complex flow field of forward flight.

Although reflex cambered profiles have an earlier stall than those with positive camber, it was thought likely that they could be used inboard without adverse effect on the maximum performance of the helicopter. This is because in hovering flight the inboard incidences of a normally twisted blade are below the stalling level. Also in high speed flight, inboard incidences are generally well above stall on the retreating blade, that is, in the range of azimuth that is critical for the remainder of the blade.

In the tests now described leading edge roughness was used to produce a reduction of stalling incidence and the associated reduction in maximum lift coefficient to represent changes in these quantities incurred by profiles with reflex camber. By extending the roughened regions of the blade in stages from the blade root outwards (Fig 1) and measuring the control load levels at each stage, a point can be found at which there is a rise in the pitching moments associated with an extension of the critical areas of blade stall in high speed flight.

In the second objective, the maximum lift coefficient requirements near the tip are explored in terms of a compromise between the demands of the retreating side for more camber and greater thickness and those on the advancing side for a thin uncambered section to give less drag, less noise and smaller control loads. By choosing a roughness size which causes only a small reduction in the maximum lift coefficient, and by applying a band of roughness to the leading edge of a small length of the blade only (Fig 1), the parts of the tip region which are most sensitive to a reduction in stalling incidence can be found from measurements of control loads as before. By implication these are the parts of the blade where the highest lifting ability is required to improve the performance of the rotor. This information can guide the choice and distribution of profile, chord length and twist to optimise performance.

The precise extent of the regions of separation on the blades is closely related to the perturbations in the downwash field caused by the trailing vortices which lie near the plane of the rotor. The resulting rapid changes of local incidence and steep radial loading gradients produce regions of separation which traverse rapidly along the blade. Two-dimensional prediction methods become inadequate in these circumstances and comprehensive wind-tunnel tests on a complete model comprising rotor and fuselage or, flight test measurements as described here are necessary to validate and extend rotor performance estimates.

2.1 Blade modifications and instrumentation.

Two of the four blades had previously been modified at the tip to make comparative performance measurements of two aerofoil sections[1]. The roughness in the form of grit on double-sided adhesive tape was applied to the two opposing unmodified blades. The use of a non-standard rotor system is not thought to affect the conclusions drawn.

The large and small grit sizes used were estimated from previous flight and tunnel tests to reduce the maximum lift coefficient by approximately 20% and 10% respectively in the range of Mach numbers and Reynolds numbers found on important parts of the blade.

The blade pitch links were strain-gauged, the output being indicative of blade torsional loading.

2.2 Test conditions.

An important consideration when planning the tests was that the range of rotor disc incidence should be comparable with future designs since the radial loading distribution depends not only on the speed of the helicopter but also on rotor disc incidence which is determined by the magnitude of the drag of the helicopter. Simple vector addition of flow relative to the blade shows that the local inflow reduces local blade incidence to an increasingly greater extent towards the blade root, whereas the cyclic and collective pitch change incidence equally at all radial positions. Hence, for a helicopter with a large drag, the retreating blade tip regions have relatively high incidences and are required to generate a larger share of the lift. During some of the tests a range of descending flight was included to offset the relatively high fuselage drag (by modern standards) of the Wessex and to reduce disc incidence.

2.3 Summary of control load signatures.

To provide a datum the control loads for two successive revolutions with unroughened blades are shown in Fig 2. The 100% pitch link load limit indicated is somewhat arbitrary and represents the oscillatory load giving the infinite fatigue life for the link.

Before discussing this particular figure and others, the measured control load waveforms can be interpreted more easily if they are viewed as the addition of several different disturbances to the control system. Three distinct features can be identified after examining the many differing control load waveforms, and each can be associated with blade stall at a given radial position, and at a given azimuth angle. These distinctions are arbitrarily defined for the purpose of interpreting the waveforms more easily, and indeed, as different rotor thrust coefficients and advance ratios are investigated, it will be seen how one 'feature' can merge continuously into another.

(a) Retreating blade oscillatory disturbance

For the unroughened blades the control load limit is eventually reached when blade stall gives rise to oscillatory loads, occurring at the frequency of the first torsional mode, as the blade traverses the retreating side of the rotor

disc. The azimuth position of the onset of the disturbance and its rate of growth depend on advance ratio and thrust coefficient, but usually several cycles of the oscillation are present, gradually growing in amplitude, before the motion is abruptly damped around azimuth zero. This type of disturbance is also characteristic of blades roughened in the 0.80 to 0.90 radius region, as well as for unroughened blades.

(b) Disturbance at front of rotor disc

For blade roughness configurations where the blade is roughened inboard, a disturbance due to blade stall not normally found on the Wessex helicopter, appears around the front of the rotor disc, at around 180° azimuth. It takes the form of an isolated nose-down disturbance to the blade, but does not start a persistent oscillation. The advance ratio for the onset of this disturbance correlates with the vortex crossing at approximately 180°.

(c) Disturbance at rear of rotor disc

A third feature which may be distinguished, is a rapid onset of the blade torsional oscillatory load late in the azimuth cycle. Although this is really a special case of the general torsional oscillation of the retreating blade, it is distinguished by its rapid growth to a large amplitude within one cycle. This disturbance is evident in conditions where roughness is applied near the extreme tip region of the blade, and may be associated with the stall in this region brought on by the combination of this roughness and the high blade incidences induced by wake interaction.

Returning to Fig 2 the waveforms shown are typical of the smooth blade control loads. There is an oscillation at approximately six times the rotational frequency which is superimposed on the basic once per revolution variation and this oscillation is present throughout almost the whole cycle. It is assumed that this frequency of variation of the control load is associated with torsional oscillations of the blade/control system in the first mode. The trend to note from this sequence of traces is the reduction in the amplitude of this oscillation as rate of descent is increased. This type of oscillation, type (a), frequently occurs in combination with other disturbances to the blade, but it is universally true that, when present, rate of descent always reduced its amplitude. It may be deduced that this disturbance is driven by the pitching moments developed on stalled areas of the blade fairly near to the tip, and the redistribution of loading accompanying a reduction in disc incidence alleviates this problem. When the oscillations grow sufficiently large to limit the speed of the aircraft, they become largest in the region of azimuth near 360°, but it is interesting to note that the oscillations are continuous after about 140°.

The addition of roughness inboard on the blade brings into play the type (b) disturbance at the front of the rotor disc. This special feature which is associated with the vortex crossing position, is shown in the example in Fig 3. The first three waveforms at the top of the page show the gradual onset of this disturbance as forward speed is increased in level flight for the condition where the blade leading edge is roughened from the blade root to 0.6 radius. Forward speed is further increased in the lower two waveforms, but for these cases rate of descent is required, first to avoid the level flight power limit and then for the

highest speed, to keep the total peak-to-peak amplitude below the maximum by suppressing the retreating blade oscillation. Note however, that in this case the disturbance at the front of the disc continues to grow as speed is increased.

The conditions which give rise to this disturbance at the front of the rotor are summarised in Fig 4. Curves are plotted from the measured data to show the roughness extent and forward speed combinations which coincide with the onset of this disturbance in the control load waveform. Values of the rotor thrust coefficient and rotational tip Mach number are constant for each curve. The disturbance becomes increasingly large in areas of the graph to the right of each boundary.

As the waveform examples have shown, these boundaries in Fig 4 confirm that increasing forward speed eventually gives rise to this disturbance, and that the speed at which it is first apparent is reduced as the roughness is gradually extended from the blade root. As anticipated, the higher mean blade loadings at a high thrust coefficient give rise to an earlier onset of the disturbance, and for regions towards the blade tip, the sensitivity of the aerofoil performance to Mach number is revealed by the separation of the boundaries beyond 0.7 radius.

The shape of each of these boundaries also reveals something of the loading along the blade at this azimuth position. The incidence distribution depends on the trim of the whole rotor, which in turn will depend on the performance limitations of the blade at other azimuth positions, but it seems certain that there is a region near the root where the addition of roughness will produce little change in the boundaries. Similarly, near the blade tip, if the general incidence level is well below the stall at 180°, further extension of the roughened region will produce no change in the value of advance ratio for the onset of the disturbance. Hence the vertical trend of the boundaries in these two regions.

The most interesting part of these boundaries is the central region, where the progressive increase in the radial extent of the leading edge roughness begins to reduce the speed for the onset of the disturbance. The straight line drawn diagonally across Fig 4 defines the estimated radial location of the tip vortex from the previous blade in the absence of wake distortion at the front of the rotor disc. To aid visualisation a sample tip vortex pattern is shown in Fig 5. Roughening the blade has little effect on the onset of this disturbance until the portion of the blade above this line, which is influenced by the upwash from this trailing vortex, is roughened.

Both the changes in the mean inflow and the local flow perturbations in this region due to the displacement effect of the fuselage will cause an increasing share of the load to be taken inboard on the blade as speed is increased, contributing to the trends shown by these boundaries. However, the position of the onset, and the rapid growth of this disturbance to quite a large amplitude indicates that it is the roughness, causing the blade to stall in the highly loaded region affected by the vortex upwash, which is the primary cause of this disturbance, rather than a more gradual extension of an inboard stalled area out along the blade. If a change of pitching moment coefficient with stall of 0.15 is assumed, this would require approximately four chord lengths of the blade to be stalled in the localised region of upwash, which is consistent with the interpretation of events described. Note that the dashed portion of the curve (Fig 4) for the lowest Mach number is for a measurement in descending flight. The oscillatory behaviour of

the retreating blade dominates the waveform shape at these advance ratios and it is only the suppression of this oscillation by rate of descent, that allows the presence of the disturbance at the front of the disc to be detected. It is a very weak disturbance as the vortex has moved far inboard at this speed, and at higher advance ratios it is expected to disappear altogether.

Examples of the third main feature of the control load waveform, type (c), occurring with a small band of roughness near the tip are presented in Fig 6. This is the large upward-going excursion in the load which appears just before zero azimuth position. Fig 6 illustrates the onset and growth of this disturbance. Although not illustrated here, like all the disturbances which are attributable to regions of the blade towards the tip, it is alleviated by increasing rate of descent as more of the load is taken inboard. This disturbance contributes substantially to the total oscillatory amplitude because it adds to the basic first harmonic (once per revolution) variation in control load. For the Wessex helicopter the first harmonic has a peak nose-down excursion in the azimuth region of 180°, which contributes to the total disturbance at 180°, and similarly at azimuth zero, the peak nose-up excursion of the first harmonic adds to this brief oscillatory disturbance. For rotors where the concern is a fairly large first harmonic variation of pitching moments due to blade camber, the phasing of these disturbances might appear to be less significant.

2.4 Overall amplitude of oscillatory load.

The quantity used to define the magnitude of the control loads is the peak-to-peak value of oscillatory load, that is the difference between maximum and minimum load in any one revolution averaged over several revolutions of the rotor. These values of oscillatory load in level flight are shown against advance ratio for various lengths of inboard roughness in Fig 7. The rotor thrust coefficient and rotational tip Mach number are constant. The roughness as far as 0.4 radius makes little change to the control loads, but beyond this point, for example for the roughness applied to 0.6 radius, there is an appreciable rise in the control loads at high advance ratios. At first the advance ratio is limited to 0.3 in level flight by the engine power available, but when the roughness is extended to 0.7 radius and beyond, the requirement to keep the total amplitude of the oscillatory loading below a maximum level set for this aircraft means that the maximum permissible forward speed has to be reduced. In the worst case, when all the blade leading edge is roughened, the maximum speed has to be restricted to 60% of that determined by the power limit.

It is significant that the shape of these curves differs from the usual control load curves characteristic of the Wessex helicopter. Instead of the somewhat constant level of loads at moderate speeds, followed by a rather rapid rise as the limiting conditions are approached, there is an early rise in loads to a higher level than for smooth blades, which is then followed by the usual rapid rise as the limit is reached. This 'bulge' in the curves is especially apparent in the curves for roughness to 0.7 radius and 0.8 radius, and analysis of the control load waveform shows how it is caused by a disturbance at the front of the rotor disc (type b) initiated by the blade roughness. However, it is the subsequent steep rise at the end of the bulge which eventually leads to the limiting load.

An appreciation of the severity of the increase in loads for each length of roughened blade near the tip can be obtained from Fig. 8. The peak-to-peak amplitudes

are plotted against the location of the 5% roughness band, and the results for each descent rate arranged on a composite graph. The dotted lines show the load levels for smooth blades at each descent rate. In this form it can be clearly seen, that the roughness around 0.9 radius produces the largest increases in control loads for level flight and moderate descent rates, but the situation changes at higher descent rates, roughness around 0.8 radius producing the largest increase in loads at the highest descent rate.

2.5 Principal conclusions of controlled roughness tests.

The measurements suggest that if profiles with reflex camber, resulting in this instance in a reduction in $C_{L\ max}$ of 0.2, were used on the inner portion of the Wessex blade to offset pitching moments from high lift sections nearer the tip, their use beyond 0.4 radius would lead to the premature onset of control load disturbance at the front of the rotor disc. If used beyond 0.6 radius, the effect of this disturbance would be large enough to necessitate a limit on speed of the Wessex helicopter. By revealing the nature of this disturbance these results provide a means of estimating the significance of this limitation for future designs where sections with increased maximum lift coefficient and pitching moment could be used to advantage in the tip region but in combination with different control system strength, number of blades and twist distribution, fuselage layout and rotor clearance.

Since these tests were made the raising of the rotor in both UTTAS designs suggests rotor-fuselage clearance may well play an important part in this type of disturbance. The design trend of bulky fuselages with a larger forward protrusion and resultant upwash over the nose into sensitive areas of the rotor adds to the problem.

In investigating the tip region of the rotor blade, the onset of the retreating blade oscillations, which eventually generate the limiting control loads, has been found to be particularly dependent on the performance of the blade profile between 0.8 and 0.9 radius. Reductions of maximum lift coefficient even nearer to the blade tip create large control load disturbances at the rear of the rotor disc. However, in general terms, sensitivity at each radial position is very dependent on blade-wake interaction which varies with advance ratio, and also with overall radial load distribution governed by rotor disc incidence.

3 PROPAGATION OF STALL IN THE TIP REGION

As mentioned in the introduction a comprehensive series of pressure measurements have been made in the blade tip region of the Wessex helicopter. A principal objective in the analysis has been the investigation of aspects of stall which may not be fully represented in two-dimensional aerofoil tests, steady or oscillatory. The aim is to define the main features of the pressure distribution to provide a basis for a theoretical model of the stall taking into account the simultaneous radial and chordwise variations of pressure.

The pressure distributions were measured using a number of absolute pressure sensors mounted in a fairing near the blade tip, locally modified to RAE 9615 section. In addition to the detailed chordwise distribution at 0.92R, sensors along the leading and trailing edges give an indication of incidence and stall at adjacent chordlines. This technique is discussed in more detail in section 4.

Roughness was again applied to the blade leading edge for this particular experiment so that substantial blade stall could be obtained near the tip at a moderate advance ratio within the flight envelope.

Blade stall may occur at differing azimuth and radial positions depending on the rotor thrust coefficient, advance ratio, and the torsional response of the blade, but it is also influenced by the incidence change induced by the passage of the tip vortex from the preceding blade. Fig 10 illustrates the relative position of the blade and tip vortex at three azimuth angles for an example which has been chosen to illustrate particular characteristics of the stall mechanism.

The indicator sensors spaced along the blade leading edge reveal that the stall progresses outwards along the blade at the same rate at which the vortex crossing point moves towards the tip. It is assumed that the local incidence distribution associated with this vortex crossing does not change significantly in the time taken for the stall to pass across the chordwise array of pressure sensors. These sensors effectively scan the edge of the stalled region and can be used to describe the structure of the stall boundary which essentially retains the same form as it traverses along the blade.

3.1 Time and spatial history of stall.

The measured force and moment coefficients at 0.92R are shown in Fig 11 for one revolution of the rotor together with corresponding chordwise pressure distributions at significant azimuth positions. On the retreating blade the normal force coefficient C_N climbs to a value of 1.14 and then the blade stalls at this radius. Following the passage of the vortex from the preceding blade, the local incidence is reduced and the section becomes unstalled, only to stall again as incidence rises during the torsional oscillations which follow the initial blade stall (this torsional instability being revealed by the control load measurements). The stages in development of the chordwise pressure distributions in this complex situation produced by a combination of vortex induced stall and torsional oscillations are shown in (a) to (h) of Fig 11.

As far as azimuth 240° (a), the chordwise distributions resemble those during a progression of increasing incidence in steady two-dimensional flow, but from 246° onwards when the chordwise force reaches its lowest value, the suction peak becomes broader, until the distribution shown at 250° (b) develops. Here the maximum nose-up pitching moment is generated, but then the suction near the nose of the aerofoil begins to fall, and after 254° the lift stall begins and progresses until at 270° (c) the whole of the suction peak has gone, and the section generates a considerable nose-down pitching moment. This state continues until after the vortex from the previous blade has passed this radial position and the incidence reduction enables the suction peak to begin re-establishing itself at about 290° (d). After this however incidence rises again because of the blade torsional motion and the chordwise pressure distribution repeats a similar cycle of events with the leading edge suction growing to a peak at 307° (e) the lift then increasing further as the suction peak becomes wider until stall again occurs at 315° (f). The stall is not so severe in this cycle and after reaching a peak nose-down pitching moment at 330° (g), the leading edge suction is re-established and the pressure distribution resembles a normal steady two-dimensional shape again by 345° (h). It is important to note that the pressure distributions and the force and moment coefficients follow

essentially the same sequence in each cycle. The feature to consider now is the rate at which these pressure disturbances spread in both chordwise and radial directions.

Figure 12 shows a composite plot of the outputs of the upper surface sensors along the chordline at 0.92 radius. The onset of the first stall is indicated by the departure from a smooth variation of the pressures around the azimuth, and the two stall cycles are revealed by the two successive waves in the pressure near the leading edge. A line has been drawn across the set of curves to define the progression of the disturbance across the chordline as the blade rotates. Similarly in Fig 13 the pressures measured at four radial positions near the blade leading edge have been superimposed to trace the progression of the disturbances in a radial direction. Again the diagonal line defines the onset of the first stall cycle. The stall progresses radially outwards along the blade at approximately the same rate as the vortex crossing traverses radially (Fig 10) as would be expected since the local incidence distribution is associated with the rotational velocities of the vortex. Since the main features of this incidence pattern do not change radically, but simply move outwards along the blade, the chordwise pressure distributions in Fig 11 scan successive cross-sections of a "stall front" which is moving along the blade and which will only change slowly as it reaches different radial positons. The diagonal line on Fig 9 indicates the approximate inclination of this "stall front" as it passes 0.92 radius. Note that the inclination to the chordline is much greater than that of the local free stream flow direction at this azimuth.

The second stall cycle presents a somewhat different radial pressure distribution although the sequence of pressure distributions at 0.92 radius resembles that of the first cycle. The second stall cycle affects only the extreme tip of the blade (Fig 13) the incidence changes being caused by the blade dynamic twist superimposed on a basic incidence pattern which rises towards the tip due to the trailed vortices lying just beyond the tip at this azimuth position. Once more, the chordwise pressure distributions (Fig 11) at 0.92 radius show a cross-section of the stall front which lies across the blade. This time the width of the suction peak grows to be very much greater than during the first stall cycle. The distinction to be made here is that whereas in the first stall cycle the front progressed radially along the blade, in this second cycle the nature of the incidence change creates a local separation which grows in strength then disappears again as shown by the simultaneous onset of the stall in Fig 13. The similarity of the successive chordwise distributions (Fig 11) in each cycle suggests that the nature of the three-dimensional flow at the edge of the stalled region is not greatly influenced by the rate of movement radially along the blade.

3.2 Discussion.

It is appreciated that many unsteady effects can contribute to the detailed nature of stall on a rotor blade and this example is considered to be representative of a "typical" case. No attempt is made here to test the validity of the various available prediction methods which are usually based on two-dimensional measurements or theoretical models of the flow, but it is interesting to observe that the delay between the initial lift and pitching moment breaks (Fig 11) is much smaller than the value predicted by Beddoes[4], although other flight cases fall nearer to the predicted value. Also the rate of chordwise propagation of the initial disturbance in the first cycle compares closely with the values measured by Carta[5] in two-

dimensional oscillatory test conditions, strengthening the similarity between the essentially three-dimensional flow on the rotor blade and measurements of this type.

4 MEASUREMENTS OF RADIAL DISTRIBUTION OF "INCIDENCE" AND STALL USING THE PUMA

The principal objective of the tests is to obtain aerodynamic, structural and dynamic behaviour to check prediction methods with the emphasis on the detailed radial distribution of stall. This is considered important because previous experimental work has not always given the definition and detail to assess the three-dimensional nature of stall and its onset in the environment of the helicopter rotor. Because of limitations on the number of measurement channels available the local aerodynamics were characterised by two features only ie leading edge and trailing edge pressures.

The surface pressures at 0.02C upper surface may be thought of as "incidence" indicators up to stalling incidence although of course their "calibration factors" are a function of Mach number. The surface pressure coefficients at a similar chordwise position obtained from two-dimensional wind tunnel tests are shown in Fig 14. It will be seen that at $M = 0.6$ and below, corresponding to conditions in the retreating blade sector the slopes of the curves are reasonably similar. The 0.02C pressures may also be considered to be representative of leading edge peak suction the collapse of which is the prelude to stall. A somewhat improved "incidence" indicator can be obtained using differential pressure between upper and lower surfaces but this was impracticable because of the difficulty of mounting transducers in the main spar of the blade.

The surface pressures at 0.91C are primarily "stall" indicators. This technique has been used successfully in previous flight tests with pressure divergence coefficients of 0.3 or more being indicative of complete stall.

A series of two-dimensional wind tunnel oscillatory aerofoil tests is currently being carried out which includes pressure taps at similar chordwise positions. This work will help in identifying unsteady aerodynamic effects and should it prove difficult to correlate leading edge pressure with incidence directly it will be a convenient parameter on which to compare flight and tunnel results.

To aid interpretation a crude chordwise pressure distribution (5 upper surface pressure transducers) at 0.8R is also included with a closer grouping of leading and trailing edge pressure transducers either side.

The blade with pressure transducers is also strain-gauged giving flap, lag and torsional bending moments at a number of radial stations ie 8, 2 and 2 respectively.

The flight measurements it is hoped, will eventually enable the separate ingredients of prediction, these are: aerofoil characteristics, the rotor wake model and blade structural and dynamic behaviour, to be investigated and compared.

4.1 Blade modifications.

The position of the pressure transducers (absolute pressures) and the method of burying them where necessary in the main spar is shown in Fig 15. The emphasis

has been to maintain an unmodified profile (NACA 0012). The anti-erosion nose strip has been retained and the only small protrusions are the thin bands of wires conducting the signals to the hub on the underside of the blade about the quarter chord.

Extensive fatigue tests were made by SNIAS prior to the flight tests. Various critical blade loads are monitored and the information is used to compute fatigue damage rates. Before modification the blade had a remaining life of 500 hours which after modification has been reduced to some 50-100 hours dependent on the type of usage.

4.2 Data reduction.

The recording and data reduction are basically similar to those developed for the Wessex although the number of data points per rotor revolution has been reduced to 256 to be accommodated within the available bandwidth.

One difficulty has been obtaining the required accuracy of the pressure coefficients at the inner radial stations where the local chordwise dynamic head is relatively small, particularly on the retreating blade. The coefficients depend on the small difference between the transducer pressures and ambient obtained from the aircraft altimeter, both being well away from calibration datums, particularly at altitude. Any constant error then appears as a periodic variation with azimuth when made into a pressure coefficient using rotor speed, blade azimuth angle, local radius and flight speed. Methods are in hand to reduce such errors.

4.3 Results.

Only the preliminary stages of a series of tests have so far been completed. Even within an extended flight envelope only limited retreating blade stall has been encountered in rectilinear flight where steady consistent results are most easily obtained. Extensive stall has been recorded during manoeuvres but this tends to be more variable and less suitable for comparison with theory. It is hoped during the next phase that the rectilinear flight envelope will be further extended.

The most commonly used results are plots of leading edge and trailing edge pressure against azimuth and these are available as multiple sensor plots or as single sensor plots on a larger scale.

An example of a multiple plot of leading edge pressure, the "incidence" indicator, is shown in Fig 16, hard copied from the Visual Display Unit. The flight condition is one of moderate advance ratio and the radial and azimuthal pattern of variation from blade-vortex interactions are well defined. The estimated blade-vortex crossings (in plan view) assuming a simple cycloidal trajectory of the tip vortex has been superimposed and show an obvious correlation with "incidence" changes but some distortion of this simple model is evident in the third quadrant.

Single sensor plots of leading edge and trailing edge pressures at a high advance ratio at the limit of the extended flight envelope, in a shallow descent, are shown in Figs 17 and 18. In Fig 17 a large leading edge pressure (peak suction) still exists at $\psi = 270^{\circ}$ and there is corresponding "noise" in the trailing edge

pressure without definite divergence. Fig 18 corresponds to conditions 3 seconds later during the gentle recovery to level flight, the increased loading has precipitated stall as evidenced by the collapse of peak suction and marked trailing edge pressure divergence.

5 CONCLUDING REMARKS

The technique of applying surface roughness systematically to portions of the leading edge of the main rotor blades to reduce the local value of the maximum achievable lift coefficient has given an insight into the requirement for tailoring blade section design in order to raise the limits of rotor performance. Some of the conclusions drawn are given at the end of section 2 and an unfavourable blade-vortex interaction is highlighted.

Examples of the detailed chordwise and radial pressure distributions have been given and the significance of three-dimensional flow discussed. Further tests are planned and a bank of relevant data is thus being built up to validate and aid the extension of prediction methods.

REFERENCES

1 M. J. Riley and P. Brotherhood, Comparative performance measurements of two helicopter blade profiles in hovering flight. ARC R&M No 3792 Feb. 1974.

2 P. Brotherhood and D.W. Brown, Flight measurements of the effects of simulated leading edge erosion on helicopter blade stall torsional loads and performance. Royal Aircraft Establishment TR 76039, March 1976.

3 M. J. Riley, A flight investigation of the spanwise lift requirements of a helicopter rotor blade by measurement of the control loads arising from locally applied roughness. Royal Aircraft Establishment TR 76117, Sept. 1976.

4 T. S. Beddoes, A synthesis of unsteady aerodynamic effects including stall hysteresis, Forum Proceedings of the 1st European Rotorcraft and Powered Lift Forum, Paper No 17, Sept. 1975.

5 F. O. Carta, Analysis of oscillatory pressure data including dynamic stall effects. NASA CR-2394, May 1974.

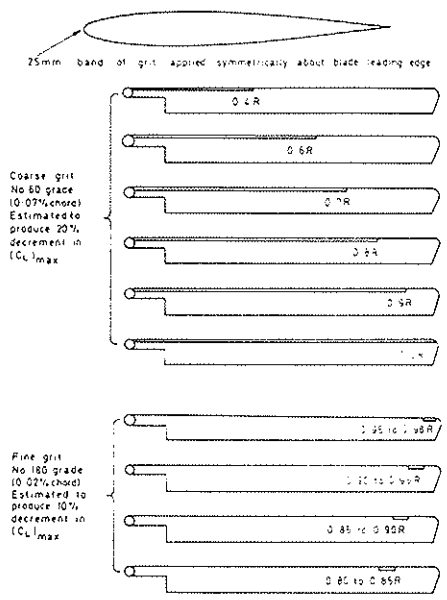

Fig 1 Leading edge roughness configurations

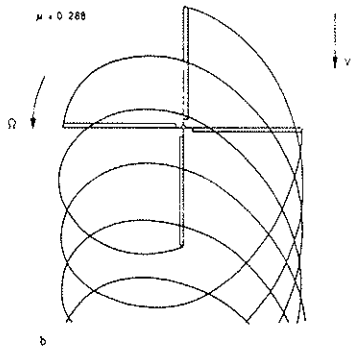

Fig 5 Example of undistorted tip vortex paths in forward flight

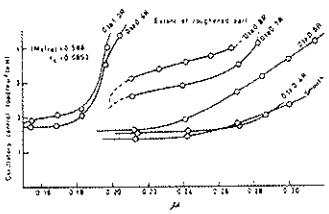

Fig 7 Peak-to-peak amplitude of oscillatory control loads in level flight

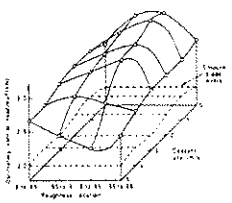

Fig 8 Variation of control load with roughness location for a range of descent rates at $\mu = 0.3$

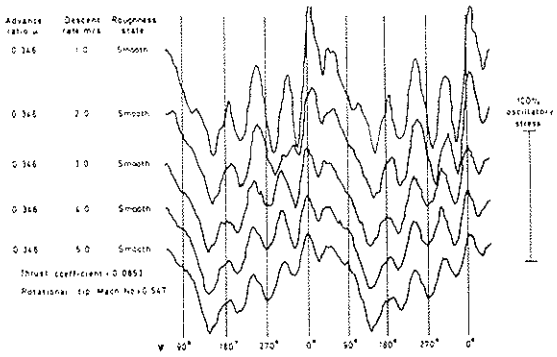

Fig 2 Torsional oscillation of retreating blade with un-roughened blades

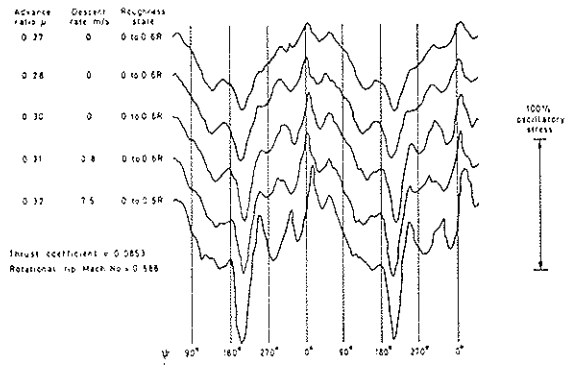

Fig 3 Disturbance at front of rotor disc caused by roughness from blade root to 0.6 radius

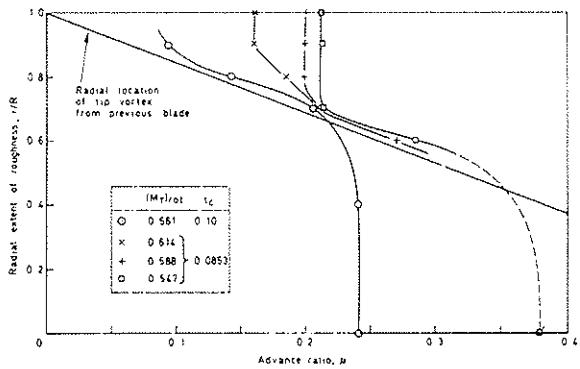

Fig 4 The onset of the disturbance at the front of the rotor disc in level flight

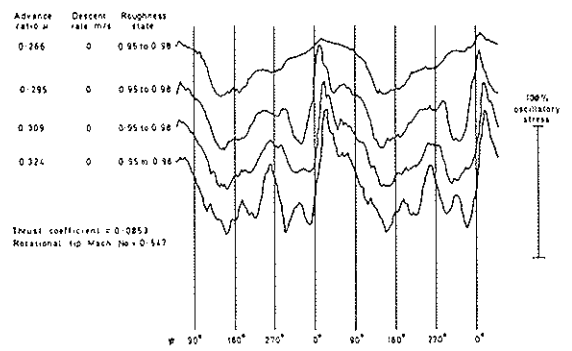

Fig 6 Disturbance at rear of rotor disc caused by roughness near blade tip

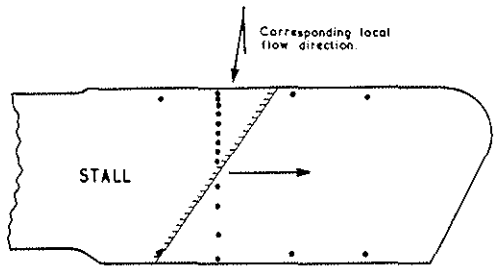

Fig 9 Sensor locations and position of stall front

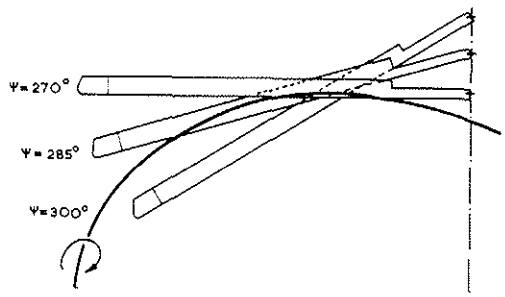

Fig 10 Position of tip vortex from previous blade

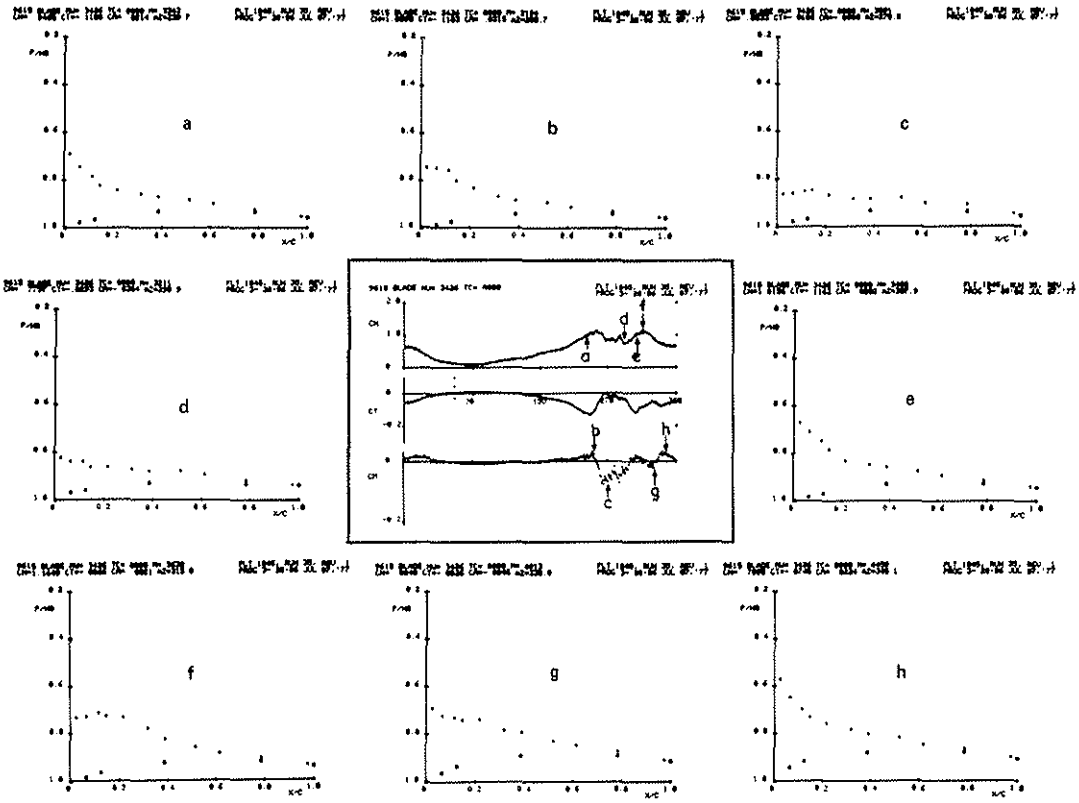

Fig 11 Force and moment time histories with associated chordwise pressure distributions

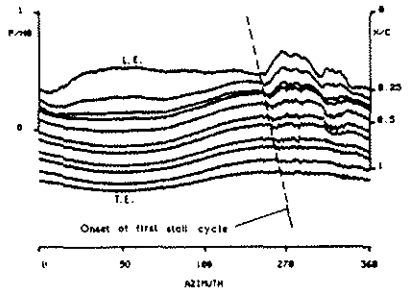

Fig 12 Pressures at intervals along the chordline at 0.92 radius

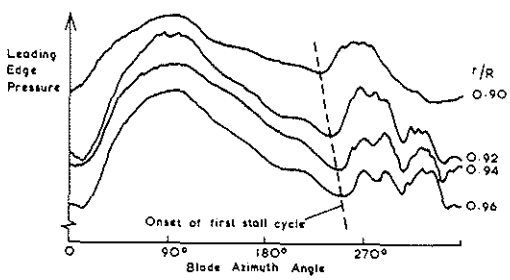

Fig 13 Pressures along the blade leading edge

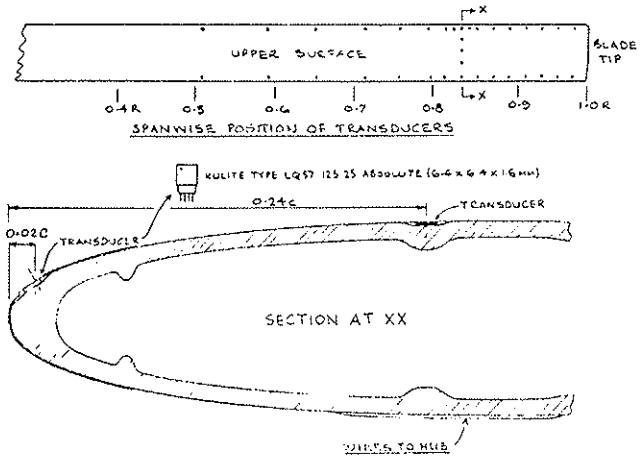

Fig 14 Puma blade instrumentation

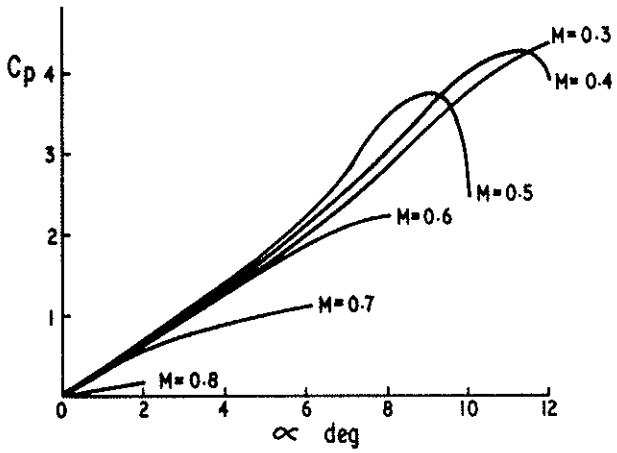

Fig 15 Upper surface, 0.02C, pressure coefficient for NACA 0012 transition fixed

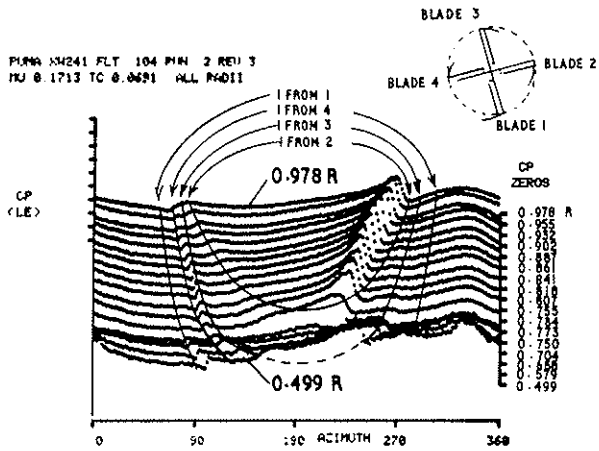

Fig 16 Leading edge pressure coefficients ("incidence") with possible undistorted tip vortex intersections superimposed

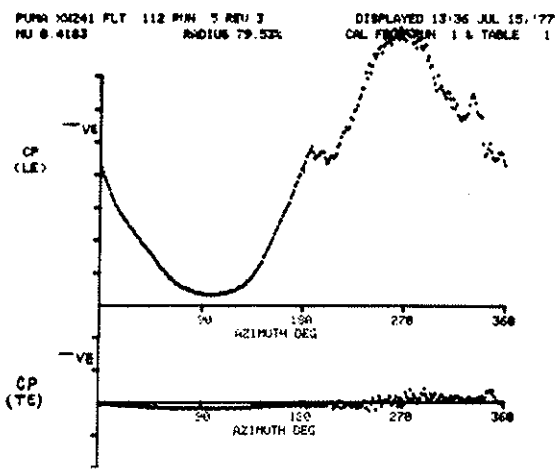

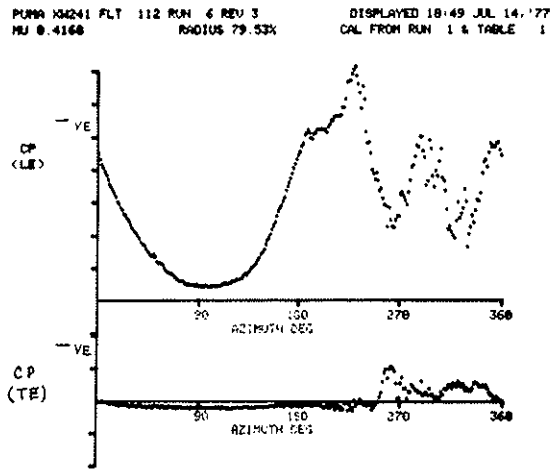

Figs 17 & 18 Leading and trailing edge pressures, before stall (Fig 17), and after (Fig 18)